IET Control Theory & Applications

The Institution of Engineering and Technology

Mechanical Sensorless LPV torque ripple control of Hybrid Electric Vehicle

ISSN 1751-8644
doi: 0000000000
www.ietdl.org

Sebastien Cauet[1], *Erik Etien*[1], *Laurent Rambault*[1]

[1] *University of Poitiers, LIAS-ENSIP Laboratory, 2 rue Pierre Brousse, 86073 Poitiers, France,* ✉ *E-mail: sebastien.cauet@univ-poitiers.fr*

Abstract: This research concerns the vibration reduction transmitted by the thermal engine to the drivetrain. In the context of a hybrid electric vehicle, the use of an electric synchronous machine, more specifically a permanent magnet synchronous machine, is recommended to partly ensure vehicle propulsion but also to mitigate the torque pulsations generated by the engine. Most strategies using this propulsion method require a very accurate position sensor. However, instead of using a sensor, this research proposes the use of a position/speed observer. This approach is combined with linear parameter varying control to guarantee consistent performance during speed transients. Thus, this strategy does not use additional hardware for a hybrid drive and consumes very little additional electrical energy (excluding the electrical losses in the motor and the inverter). These methods are illustrated within the context of an urban trip and clearly show the effectiveness of the proposed approach.

1 Introduction

Many countries have implemented policies to significantly reduce emissions of greenhouse gasses such as carbon dioxide. Automotive manufacturers have achieved these objectives by introducing solutions such as downsizing and hybridisation. Both of these solutions involve either a reduction in the number of cylinders or engine downsizing. The downsized engines then attain the required performance by operating at higher average pressure. The use of turbo-chargers allow these engines to deliver torque at levels comparable to those of conventional engines.
However, this causes undesirable side effects such as cycle irregularities, which cause torque oscillations. In the case of a hybrid electric vehicle (HEV), an additional actuator is present and offers a new degree of freedom: an electric motor (in most cases, a synchronous motor with permanent magnets (PMSM)). Here, the main objective is to use this engine for both electric propulsion and for mitigating torque oscillations.
In that case, it generates improved performance in terms of the durability of the transmission and in terms of noise without increasing the fuel consumption and degrading the effectiveness, as shown in [1]. Several approaches have been followed to reduce the torque oscillations and vibration in flexible structures: examples are stiffening, isolation, and damping [2]. Among these solutions, damping is most commonly used. From an energy point of view, there are two methodologies: passive and active.
Passive solutions often use inertia, whereas active solutions use an external energy source to act in the vibration peaks.

Several studies that have focused on techniques to achieve these active solutions in HEVs have been reported in the literature. The first solution, which is based on the use of an alternator and is effective at both steady and idling speed, was published in [3]. In [4], the torque oscillations are reduced in an open loop. Approaches with observers [5] and those based on neural networks [6] were also implemented. An approach using PID and notch filters has been proposed [7]. More recently, three approaches, i.e. H_∞ [8], LPV [9] and MPC [10], which limit the maximum torque of the electric motor, were proposed. Additionally, a torque split strategy was employed in combination with an automated mechanical transmission (AMT) gear-shifting strategy [11].

In [12], the authors present three different solutions for a torque damping control system, i.e. a conventional proportional integral controller, an observer-based torque feed-forward technique, and an original approach based on an adaptive multi-resonant controller. In the case of electric vehicles, other authors, [13], proposed a generalised real-time suppression strategy to mitigate the coupling vibration during vehicle idling and cruising. The use of a high-performance field oriented controlled (FOC) electric motor drive enables a relatively small amount of rotation velocity offset to be added to the traction motor to significantly reduce the resonant vibration with negligible impact on the vehicular speed. Other solutions can be implemented in a wide range of applications, e.g. active ripple compensation has been applied in domestically combined heat and power [14]. However, all these approaches require precise and expensive instrumentation. At a minimum, the approaches use the measurements of the angular positions and a speed sensor. This incurs additional costs and a point of mechanical weakness.

In the aforementioned work, the disturbance attenuation is performed on static operating points, and an improvement is proposed even when the speed changes (LPV control). The advantage of the methodology presented in this article is that it does not require modelling of the thermal engine because it is considered as a reference model of non-stationary multi-sinusoidal disturbances. A strategy must therefore be put in place to generate the reference trajectories. Therefore, a sensorless observer and a multi-sinusoidal dynamic estimator are used together.

The new approach presented in this paper does not rely on the use of a mechanical sensor. Indeed, a controller using a speed and position observer is used in the synchronous electrical machine (PMSM) controller. This not only ensures the control of the motor, but also the use of a software sensor for active torque oscillation compensation. In our application, the electrical motor is perfectly well known. We have therefore chosen to implement an observer based on a physical model of the PMSM. Several methods can be used, such as adaptive observers [15, 16], an extended Kalman filter [17], or approaches based on reference models[18]. In section 3, we present an adaptive observer built from the PMSM park model.

The paper begins with a comprehensive overview of the issue. In Section 3, the sensorless observer is presented. In the following section, the control torque oscillations in an HEV are described. The output regulation strategy is introduced in section 5 followed by the design of the LPV. Finally, the simulation results are shown to prove the effectiveness of the approach.

2 Problem statement

According to its principle of operation, an internal combustion engine generates torque pulsation, which often takes the form of a

This article has been accepted for publication in a future issue of this journal, but has not been fully edited.
Content may change prior to final publication in an issue of the journal. To cite the paper please use the doi provided on the Digital Library page.

sum of two torques, as shown in this relationship:

$$T_{ice} = T_p + T_i \tag{1}$$

where ice signify internal combustion engine. T_i is the torque generated by the oscillating masses and connecting rod; T_p is the combustion torque generated by the pressure in the cylinder; T_p and T_i can be mathically expressed by, see [19],

$$\begin{aligned} T_p &= P_r(\theta_{th}) \left[r\cos(\theta_{th}) + l\sqrt{1-\lambda_m^2 \sin^2(\theta_{th})} \right] \tan(\varphi), \\ T_i &= (m_a + m_p) r \omega_{th}^2 \left[\cos(\theta_{th}) + \lambda_m \cos(2\theta_{th}) \right] * \\ &\quad \left[r\cos(\theta_{th}) + l\sqrt{1-\lambda_m^2 \sin^2(\theta_{th})} \right] \tan(\varphi), \end{aligned} \tag{2}$$

where

$$tan(\varphi) = \frac{\lambda_m sin(\theta_{th})}{\sqrt{1-\lambda_m^2 sin^2(\theta_{th})}} \tag{3}$$

where θ_{th} describes the crankshaft position, ω_{th} is the crankshaft speed, $P_r(\theta_{th})$ model the upward thrust on the piston and the expression of $sin(\varphi) = -\lambda_m sin(\theta_{th})$. In this relation $\lambda_m = \frac{r}{l}$ and r and l are the lengths of the crank and the connecting rod, respectively. m_a and m_p are the connecting rod mass and the piston mass, respectively.
The fluctuating torque is illustrated in Fig.1-2 at idling speed in the cases of both one cylinder and four cylinders.

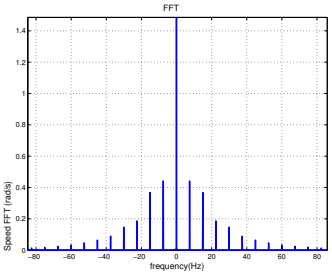

Fig. 1: Ripples Speed FFT of a mono cylinder

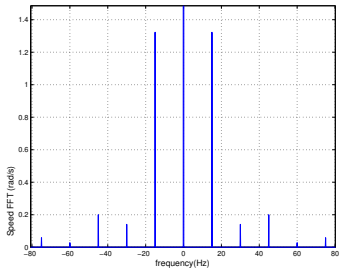

Fig. 2: Ripples Speed FFT of 4 cylinders diesel engine

Unfortunately, this pulsed torque degrades the life cycle of the drive train and reduces occupants' comfort. The addition of an electric motor on the same shaft of the internal combustion engine, as is the case in an HEV, makes it possible to overcome the undesirable oscillating torque. Indeed, the torque relationship on the shaft is:

$$T = T_{ice} + T_e - T_l, \tag{4}$$

where T_e is the electric motor torque and T_l is the load torque. Then, it is possible to attenuate the ripple torque generated by the ICE with the electrical motor torque T_e.
A global approach was followed in this paper. A block diagram representing the global overview of the sensorless active control approach can be found in Fig. 3. In the remainder of this paper,

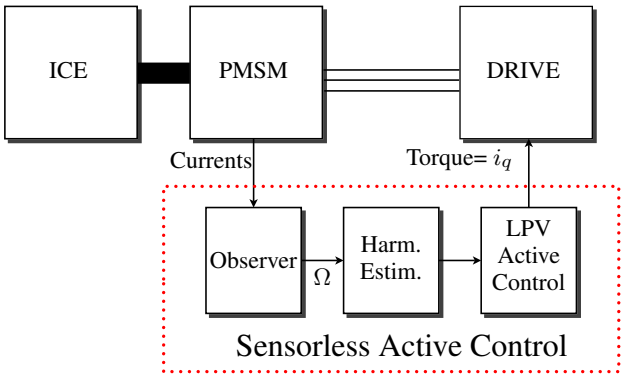

Fig. 3: Global control loop.

details of all parts of the sensorless control loop are presented. Initially, the part of the synchronous machine that is used as a sensor is introduced.
Indeed, the work focuses on a speed observer using the electrical motor current to estimate the speed and position. Then, LPV active control is implemented to remove the disturbance.

3 PMSM adaptive observer

The observers for PMSM can be described in a reference frame fixed with respect to the stator (the $\{\alpha, \beta\}$ reference frame) [20], or linked to the rotor (the $\{d, q\}$ reference frame). In the latter category, several models have been developed to obtain full [21] or reduced observers [22]. The models described in Park's paper are interesting for several reasons. First, in this reference frame, the quantities are continuous, which simplifies the design of control laws. Moreover, the linearisation of these models is simplified and makes it possible to study possible problems of convergence, stability, or design [23]. Moreover, this type of observer is particularly suitable for extending the number of quantities to be adapted (stator resistance and q-axis inductance) [24].

3.1 Synchronous motor model

First, we introduce the synchronous motor model used to configure the speed observer. In (4), the electromagnetic torque of the PMSM is part of the propulsion torque. This torque, when vector-oriented control is implemented, can be established in Park's $\{d/q\}$ reference frame fixed to the rotor as [21]:

$$T_e = \frac{3}{2} p \psi_s^T J^T i_s \tag{5}$$

where, J is a square matrix represented as:

$$J = \begin{bmatrix} 0 & -1 \\ 1 & 0 \end{bmatrix}$$

and $i_s = \begin{bmatrix} i_d & i_q \end{bmatrix}^T$ is the stator current, $\psi_s = \begin{bmatrix} \psi_d & \psi_q \end{bmatrix}^T$ is the stator flux and p is the number of pole pairs. This expression will be useful to control the motor torque.
The different equations required for the implementation of the observer are introduced to enable the synchronous motor to be modelled. First, the stator voltage equation in Park's $\{d/q\}$ is expressed

as:

$$u_s = R_s i_s + \dot{\psi}_s + \omega J \psi_s \tag{6}$$

Where $u_s = \begin{bmatrix} u_d & u_q \end{bmatrix}^T$ is the stator voltage, R_s is the stator resistance, $\omega = \dot{\theta}$ is the electrical angular speed of the rotor. In these equations, the stator flux is represented by:

$$\psi_s = L i_s + \psi_{pm} \tag{7}$$

Where ψ_{pm} is the permanent magnet flux expressed as $\psi_{pm} = \begin{bmatrix} \psi_{pm} & 0 \end{bmatrix}^T$ and L is the inductance matrix which depends respectively on the direct and quadrature axis inductances L_d and L_q.

$$L = \begin{bmatrix} L_d & 0 \\ 0 & L_q \end{bmatrix}$$

3.2 PMSM Adaptive observer

As shown in Fig. 4, the observer that is used here is an adaptive version. Indeed, initially, the observer uses as an error the difference between the observed and measured currents. Based on the model of the machine, this gap then allows the observer to be adjusted to estimate the rotor position and speed accurately.

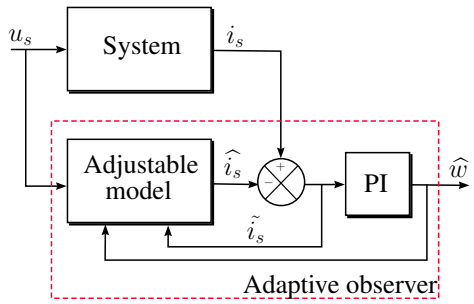

Fig. 4: Adaptive observer representation.

The adaptive observer model is based on (6) and (7) and the state space representation can be designed as [20, 25]:

$$\dot{\hat{\psi}}_s = u_s - R_s \hat{i}_s - \hat{\omega} J \hat{\psi}_s + \lambda \tilde{i}_s \tag{8}$$

The different superscript $\hat{}$ represents the estimated quantities. The error equation of the estimated stator currents can be written as:

$$\hat{i}_s = L^{-1} \left(\hat{\psi}_s - \psi_{pm} \right) \tag{9}$$

$$\tilde{i}_s = i_s - \hat{i}_s \tag{10}$$

The feedback gain matrix is λ, the design of which was determined by the following expression:

$$\lambda = \lambda_1 I + \lambda_2 J \tag{11}$$

where I is the identity matrix. In that case, the gain λ_1, λ_2 is chosen such that a pole placement is made in the complex plane. Fast observer dynamics compared to those of the current loop can be obtained by an appropriate selection of λ_1 after determining the roots of the characteristic equation of the observer model (6).

In the case of several variations, the observer can be adapted by designing the PI controller with respect to this equation:

$$\hat{\omega} = -k_p \cdot \epsilon - k_i \int \epsilon \cdot dt \tag{12}$$

where k_p and k_i are coefficients of the PI regulator. The rotor position $\hat{\theta}$ is the integrating part of the rotor angular speed. The current error ϵ is evaluated from this error equation:

$$\epsilon = \begin{bmatrix} 0 & L_q \end{bmatrix} \cdot \tilde{i_s} \tag{13}$$

4 Harmonics Hybrid Torque Control

The originality of the approach presented here, is to use a synchronous motor as a pulsating torque generator to counteract the disturbance generated by the engine. In this case, control is exercised by injecting a current reference iq_{ref} in the PMSM. In the HEV configuration, the electric motor is then regarded as the producer of torque control. In this case, the internal combustion engine acts as a generator of unsteady and multi-sinusoidal external disturbance. The proposed approach ignores the nonlinear model (2) of the torque generated by the engine. In this study, the ICE is considered as an exogenous disturbance. Thus, the problem becomes a generalised asymptotic regulation problem, as seen in [26]. Thus, the control objectives are intended to assure quadratic stability while ensuring the mitigation of ICE torque ripples. The systems Σ can model the electromechanical system that is used to design the LPV controller:

$$(\Sigma) : \begin{cases} \dot{\mathbf{x}} = \mathbf{A}\mathbf{x} + \mathbf{B_w}\mathbf{w} + \mathbf{B_u}\mathbf{u} \\ \mathbf{y} = \mathbf{C_y}\mathbf{x} + \mathbf{D_{yu}}\mathbf{u} \end{cases}, \tag{14}$$

where $\mathbf{x^T} = [\theta_{th}, \omega_{th}, \theta_e, \omega_e] \in \mathbb{R}^n$ is the state vector ($_{th}$ stands for thermal engine, $_e$ for electrical motor), $\mathbf{u} \in \mathbb{R}^{n_u}$ is the control input vector (PMSM current i_q), $\mathbf{w} \in \mathbb{R}^{\mathbf{n_w}}$ is the exogenous disturbance which will be defined afterwards, $\mathbf{y} \in \mathbb{R}^{\mathbf{n_y}}$ is the controlled output vector (the diesel engine speed).

The matrices involved in (14) can be defined as follows:

$$\begin{aligned} \mathbf{A} &= \begin{bmatrix} 0 & 1 & 0 & 0 \\ \frac{-k}{J_1} & \frac{-c}{J_1} & \frac{-k}{rJ_1} & \frac{-c}{rJ_1} \\ 0 & 0 & 0 & 1 \\ \frac{k}{rJ_2} & \frac{c}{rJ_2} & \frac{-k}{r^2 J_2} & \frac{-c}{r^2 J_2} \end{bmatrix} \mathbf{B_u} = \begin{bmatrix} 0 \\ 0 \\ 0 \\ \frac{3}{2}\frac{p\lambda}{J_2} \end{bmatrix}, \\ \mathbf{B_w} &= \begin{bmatrix} 0 & 0 & \cdots & 0 & 0 \\ 0 & \frac{1}{J1} & \cdots & 0 & \frac{1}{J1} \\ 0 & 0 & \cdots & 0 & 0 \\ 0 & 0 & \cdots & 0 & 0 \end{bmatrix} \mathbf{C_y} = \begin{bmatrix} 0 \\ 1 \\ 0 \\ 0 \end{bmatrix}^{\mathbf{T}} \\ & \quad \underbrace{\qquad}_{B_w^1} \qquad\qquad \underbrace{\qquad}_{B_w^\eta} \\ \mathbf{D_{yu}} &= \mathbf{0_{n \times n_u}} \end{aligned} \tag{15}$$

where k is the stiffness; c is the damping coefficient; r is the ratio between the PMSM (permanent magnet synchronous motor) and diesel engine shafts; J_1 is the ICE inertia mass moment; J_2 is the PMSM inertia mass moment; p is the number of pole pairs of the PMSM; λ is the flux linkage per phase. θ_{th} and ω_{th} are the crankshaft position and speed respectively; θ_{el} and ω_{el} are the rotor position and speed, respectively. It is assumed that the current controller of the synchronous motor can be modelled as a first order Σ_{el}, where τ_e is the time constant of the current control loop and describes the torque control loop of the variable-frequency drive.

In (14), $\mathbf{w}(t)$ is a non-stationary disturbance generated by a multi-sinusoidal exogenous linear system. Suppose that $\mathbf{w}(t)$ represents η sinusoidal harmonics of which the frequencies are $\omega_{h_i}(t) \in [\underline{\omega}_{h_i}, \overline{\omega}_{h_i}]; i \in \{1 \cdots \eta\}$ and $\omega_{h_i}(t) = i(\omega_0)$, where ω_0 is supposed

to be the varying parameter.
Then the exosystem becomes,

$$\underbrace{\begin{bmatrix} \dot{\mathbf{w}}_1 \\ \dot{\mathbf{w}}_2 \\ \vdots \\ \dot{\mathbf{w}}_\eta \end{bmatrix}}_{\dot{\mathbf{w}}} = \mathbf{A_e}(\omega_0(t)) \underbrace{\begin{bmatrix} \mathbf{w}_1 \\ \mathbf{w}_2 \\ \vdots \\ \mathbf{w}_\eta \end{bmatrix}}_{\mathbf{w}} \tag{16}$$

where $\mathbf{A_e}(\omega_0) \in \mathbb{R}^{n_w \times n_w}$ and is given by,

$$\mathbf{A_e}(\omega_0) = \begin{bmatrix} 0 & \omega_0 & \cdots & 0 & 0 \\ -\omega_0 & 0 & \cdots & 0 & 0 \\ \vdots & \vdots & \ddots & 0 & 0 \\ \vdots & \vdots & \ddots & 0 & 0 \\ 0 & 0 & \cdots 0 & 0 & \eta\omega_0 \\ 0 & 0 & \cdots & -\eta\omega_0 & 0 \end{bmatrix}$$

5 LPV Output regulation design

5.1 Output regulation design

In this subsection, a control strategy is developed to ensure torque ripple reduction when the speed varies. Some LPV controller designs can be found in [27–29]. The objective, therefore, is to develop an LPV controller to ensure quadratic stability when non-stationary disturbance needs to be eliminated.

For the synthesis of the LPV controller, a reference model is considered to have the same model as (14). Thus, considering $\mathbf{e} = \mathbf{x_{ref}} - \mathbf{x}$ (an error system), the following representation is given:

$$(\Sigma_\Delta) \begin{cases} \dot{\mathbf{e}} = \mathbf{Ae} + \mathbf{B_w}\boldsymbol{\Delta w} + \mathbf{B_u}\boldsymbol{\Delta u} \\ \bar{\mathbf{y}} = \mathbf{C_y e} + \mathbf{D_{yu}}\boldsymbol{\Delta u} \end{cases}, \tag{17}$$

with $\mathbf{e} = \mathbf{x_{ref}} - \mathbf{x}$; $\boldsymbol{\Delta w} = \mathbf{w_{ref}} - \mathbf{w}$, $\boldsymbol{\Delta u} = \mathbf{u_{ref}} - \mathbf{u}$ and $\dot{\boldsymbol{\Delta}}\mathbf{w} = \mathbf{A_e}(\boldsymbol{\omega_0(t)})\boldsymbol{\Delta w}$. This equation models the dynamics of the non-stationary quasi-periodic disturbances. Designing a controller $K(\omega_0)$ capable of stabilising the system (17) makes it necessary to make some assumptions.

Remark 1. *In the context of this study, the limitation of the ripple of the diesel engine torque requires a reference speed trajectory to be defined. This trajectory is generated without the harmonics being completely cancelled. A recursive least squares algorithm is used to estimate this trajectory. A scalar $\kappa \in R$ is introduced to modulate the level of disturbance attenuation. In this case, the controller balances the energy consumption with the requirement of vibration attenuation.*

Proposition 1. *Consider an LPV system in which the dynamics are described by (Σ_Δ) with non-stationary disturbance, and assume that*

A.1. $\mathbf{A_e}(\boldsymbol{\omega_0(t)})$ *is anti-Hurwitz (i.e. has all its eigenvalues as non-negative real parts),*

A.2. $(\mathbf{A}, \mathbf{B_u})$ *is stabilizable (i.e.* $\exists \mathbf{F} : \mathbf{A} + \mathbf{B_u F}$ *is Hurwitz,*

A.3. $\begin{pmatrix} \mathbf{A} & \mathbf{B_w} \\ \mathbf{0} & \mathbf{A_e}(\boldsymbol{\omega_0(t)}) \\ \mathbf{C_y} & \mathbf{0} \end{pmatrix}$ *is detectable,*

The controller $\mathbf{K}(\boldsymbol{\omega_0(t)})$ *is designed such that*

A.1.(Internal Stability) The closed-loop system with the controller $\mathbf{K}(\boldsymbol{\omega_0(t)})$ *is asymptotically stable,*

A.2.(Almost Asymptotic Regulation) There exists κ such that $\|\bar{\mathbf{y}}(\mathbf{t})\| = \left(\bar{\mathbf{y}}(\mathbf{t})^{\mathbf{T}}\bar{\mathbf{y}}(\mathbf{t})\right)^{\mathbf{1/2}} \leqslant \kappa \|\boldsymbol{\Delta w}(\mathbf{t})\|, \forall t \geqslant 0$, *starting from* $\mathbf{w(0)}$.

It is necessary to introduce a term κ to change the attenuation level of the unwanted harmonics. In particular, this allows the level of the required electrical power to be reduced.

5.2 Asymptotic regulation transformation

A transformation of the problem is introduced to allow asymptotic regulation and closed-loop stability. This transformation has been inspired by ([30]).

Lemma 1. *Considering Proposition 1 and if there exists* $\mathbf{\Pi} \in \mathbb{R}^{\mathbf{n}\times\mathbf{n_w}}$ *and* $\mathbf{\Gamma} \in \mathbb{R}^{\mathbf{n}\times\mathbf{n_w}}$ *that satisfy*

$$-\mathbf{B_w} + \mathbf{\Pi A_e}(\boldsymbol{\omega_0}) - \mathbf{A\Pi} - \mathbf{B_u\Gamma}(\boldsymbol{\omega_0}) = \dot{\mathbf{\Pi}} \tag{18}$$

$$\begin{bmatrix} \kappa\mathbf{I} & -\mathbf{C_y\Pi} \\ (-\mathbf{C_y\Pi})^{\mathbf{T}} & \kappa\mathbf{I} \end{bmatrix} \geqslant 0. \tag{19}$$

$\mathbf{\Gamma}$ *and* $\mathbf{\Pi}$ *are the solutions of these above equations, named Sylvester equations see [30]. Any controller that solves this problem suggests the following expression* $\mathbf{K}(\boldsymbol{\omega_0(t)})$*:*

$$\begin{bmatrix} \dot{\mathbf{v}} \\ \boldsymbol{\Delta u} \end{bmatrix} = \left[\begin{array}{cc|c} \mathbf{A_e} - \mathbf{D_c^2}(\boldsymbol{\omega_0})\mathbf{C_y\Pi} & \mathbf{C_c^2}(\boldsymbol{\omega_0}) & \mathbf{D_c^2}(\boldsymbol{\omega_0}) \\ -\mathbf{B_c}(\boldsymbol{\omega_0})\mathbf{C_y\Pi} & \mathbf{A_c}(\boldsymbol{\omega_0}) & \mathbf{B_c}(\boldsymbol{\omega_0}) \\ \hline \mathbf{\Gamma} - \mathbf{D_c^1}(\boldsymbol{\omega_0})\mathbf{C_y\Pi} & \mathbf{C_c^1}(\boldsymbol{\omega_0}) & \mathbf{D_c^1}(\boldsymbol{\omega_0}) \end{array}\right] \begin{bmatrix} \mathbf{v} \\ \bar{\mathbf{y}} \end{bmatrix}$$

and can be implemented as, see Fig. 5

$$\mathbf{K_i}(\boldsymbol{\omega_0}) = \left[\begin{array}{c|c} \mathbf{A_e}(\boldsymbol{\omega_0}) & \mathbf{I} \\ \hline \mathbf{I} & \mathbf{0} \end{array}\right], \tag{20}$$

$$\mathbf{K_a}(\boldsymbol{\omega_0}) = \left[\begin{array}{c|c} \mathbf{A_c}(\boldsymbol{\omega_0}) & \mathbf{B_c}(\boldsymbol{\omega_0}) \\ \hline \mathbf{C_c^1}(\boldsymbol{\omega_0}) & \mathbf{D_c^1}(\boldsymbol{\omega_0}) \\ \mathbf{C_c^2}(\boldsymbol{\omega_0}) & \mathbf{D_c^2}(\boldsymbol{\omega_0}) \end{array}\right] \tag{21}$$

where $\mathbf{K_i}(\delta)$ *is a controller that replicates the dynamics of the exogenous system and* $\mathbf{K_a}(\delta)$ *is a controller that stabilises the closed loop system* (Σ_Δ)*.*

In our case and in the following developments, $\mathbf{\Pi}$ is assumed to be constant and, consequently $\dot{\mathbf{\Pi}} = \mathbf{0}$.

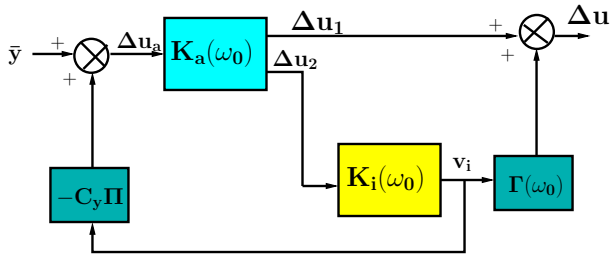

Fig. 5: Structure of the controller

This article has been accepted for publication in a future issue of this journal, but has not been fully edited.
Content may change prior to final publication in an issue of the journal. To cite the paper please use the doi provided on the Digital Library page.

Using the following transformation,

$$\tilde{\mathbf{x}} = \begin{bmatrix} \mathbf{I} & -\mathbf{\Pi} \\ \mathbf{0} & \mathbf{I} \end{bmatrix} \begin{bmatrix} \mathbf{e} \\ -\begin{bmatrix} \mathbf{0} & \mathbf{I_{n_w}} \end{bmatrix} \mathbf{v} \end{bmatrix} + \begin{bmatrix} \mathbf{0} \\ \mathbf{I} \end{bmatrix} \mathbf{\Delta w}. \quad (22)$$

the system can be expressed as,

$$\begin{cases} \dot{\tilde{\mathbf{x}}} = \tilde{\mathbf{A}}(\omega_0)\tilde{\mathbf{x}} + \tilde{\mathbf{B}}\mathbf{\Delta}\tilde{\mathbf{u}} \\ \mathbf{\Delta u_a} = \tilde{\mathbf{C}}\tilde{\mathbf{x}} \end{cases}$$

where, $\tilde{\mathbf{A}}(\omega_0) = \begin{bmatrix} \mathbf{A} & \mathbf{B_u\Gamma}(\omega_0) \\ \mathbf{0} & \mathbf{A_e}(\omega_0) \end{bmatrix}$, $\tilde{\mathbf{B}} = \begin{bmatrix} \mathbf{0} & \mathbf{B_u} \\ \mathbf{I} & \mathbf{0} \end{bmatrix}$ and $\tilde{\mathbf{C}} = \begin{bmatrix} \mathbf{C_y} & \mathbf{C_y\Pi} \end{bmatrix}$

5.3 LPV output feedback synthesis

In this subsection, the LPV problem is transformed into a polytopic description of the system in order to perform the computation using Linear Matrix Inequalities (LMIs). Other strategies exist according to which the LPV controller $\mathbf{K_a}(\omega)$ can be designed. One of the most popular is the "full block S-procedure" and the Linear Fractional Transformation (LFT) representation [31, 32]. Here, an LMI solution is preferred. In this paper, the following continuous time LPV system is considered:

$$\begin{cases} \dot{\tilde{\mathbf{x}}} = \tilde{\mathbf{A}}(\rho_\mathbf{k})\tilde{\mathbf{x}} + \tilde{\mathbf{B}}\mathbf{\Delta}\tilde{\mathbf{u}} \\ \mathbf{\Delta u_a} = \tilde{\mathbf{C}}\tilde{\mathbf{x}} \end{cases}$$

Assume that $\tilde{\mathbf{A}}(\rho_\mathbf{k})$ is a matrix which belongs to a set $\mathcal{A}$ as defined in (23). This set is a polytope of matrices and represents a convex combination of the extreme matrices $\mathbf{A_j}$, $j = 1 \dots 2^M$, referred to as the vertices of $\mathcal{A}$.

$$\mathcal{A} = \left\{ \tilde{\mathbf{A}}(\rho_k) | \; \tilde{\mathbf{A}}(\rho_k) = \sum_{j=1}^{2^M} \varsigma_i \tilde{\mathbf{A}}_\mathbf{j}, \; \varsigma_j \in \mathbf{\Delta_1} \right\}, \quad (23)$$

with

$$\Delta_1 = \left\{ \begin{bmatrix} \varsigma_1 \\ \vdots \\ \varsigma_{2^M} \end{bmatrix} \in \mathbb{R}^{2^M} | \; \varsigma_j \geq 0, \; \forall j \in 1 \dots 2^M; \sum_{j=1}^{2^M} \varsigma_i = 1 \right\} \quad (24)$$

Remark 2. *The polytope vertices are composed with the extreme values of $\rho_i \in [\underline{\rho}_i, \overline{\rho}_i]$, which are dependent on the speed ω_0.*

Let the following representation $\tilde{G}$ be introduced,

$$\left[\begin{array}{c|c} \mathbf{A} & \mathbf{B} \\ \hline \mathbf{C} & \mathbf{D} \end{array}\right] = \left[\begin{array}{cc|c} \tilde{\mathbf{A}}(\rho) & \mathbf{0} & \mathbf{0} \\ \mathbf{0} & \mathbf{0} & \mathbf{0} \\ \hline \mathbf{0} & \mathbf{0} & \mathbf{0} \end{array}\right] + \left[\begin{array}{cc} \mathbf{0} & \tilde{\mathbf{B}} \\ \mathbf{I} & \mathbf{0} \\ \hline \mathbf{0} & \mathbf{0} \end{array}\right] \underbrace{\begin{bmatrix} \mathbf{A_a}(\rho) & \mathbf{B_a}(\rho) \\ \mathbf{C_a}(\delta) & \mathbf{D_a}(\rho) \end{bmatrix}}_{\mathbf{K_a}(\rho)} \left[\begin{array}{cc|c} \mathbf{0} & \mathbf{I} & \mathbf{0} \\ \tilde{\mathbf{C}} & \mathbf{0} & \mathbf{0} \end{array}\right]$$

The accompanying controller $\mathbf{K_a}(\rho)$ can stabilise the plant $\tilde{G}$ under quadratic performance specification if there exists a symmetric positive definite matrix $\tilde{\mathbf{P}}$ in $\mathbb{R}^{n \times n_u}$ such that

$$\tilde{\mathbf{A}}_\mathbf{f}^\mathbf{T}(\rho)\tilde{\mathbf{P}} + \tilde{\mathbf{P}}\tilde{\mathbf{A}}_\mathbf{f}(\rho) < \mathbf{0} \quad (25)$$

is feasible where the matrix $\tilde{\mathbf{A}}_\mathbf{f}$ has the following definition

$$\tilde{\mathbf{A}}_\mathbf{f}(\rho) = \tilde{\mathbf{A}}_\mathbf{g}(\rho) + \tilde{\mathbf{B}}_\mathbf{g}\mathbf{K_a}(\rho)\tilde{\mathbf{C}}_\mathbf{g}, \quad (26)$$

with

$$\tilde{\mathbf{A}}_\mathbf{g}(\rho) = \begin{pmatrix} \tilde{\mathbf{A}}(\rho) & \mathbf{0} \\ \mathbf{0} & \mathbf{0} \end{pmatrix}, \tilde{\mathbf{B}}_\mathbf{g} = \begin{pmatrix} \mathbf{0} & \tilde{\mathbf{B}} \\ \mathbf{I} & \mathbf{0} \end{pmatrix},$$
$$\tilde{\mathbf{C}}_\mathbf{g} = \begin{pmatrix} \mathbf{0} & \mathbf{I} \\ \tilde{\mathbf{C}} & \mathbf{0} \end{pmatrix}.$$

Theorem 1. *Consider the problem of controller design discussed in Proposition 1. There exists a controller $\mathbf{K}(\rho)$ of the form (20) that solves this problem and achieves quadratic stabilisation, if there exists a matrix $\tilde{\mathbf{P}} \in \mathbb{R}^{\mathbf{n} \times \mathbf{n_u}}$, $\mathbf{\Gamma} \in \mathbb{R}^{\mathbf{n} \times \mathbf{n_w}}$ $\tilde{\mathbf{P}} > \mathbf{0}$, a state feedback $\mathbf{F_0}(\rho)$ that is a solution to (28), an unknown square and nonsingular variable matrix $\mathbf{G_a} \in \mathbb{R}^{\mathbf{n_u}+\mathbf{n_c}}$, an unknown variable matrix $\mathbf{L_a}(\rho) \in \mathbb{R}^{(\mathbf{n_u}+\mathbf{n_c}) \times (\mathbf{n_y}+\mathbf{n_c})}$, and two unknown variables matrices $\mathbf{F_1} \in \mathbb{R}^{(\mathbf{n_x}+\mathbf{n_c}) \times (\mathbf{n_x}+\mathbf{n_c})}$ and $\mathbf{F_2} \in \mathbb{R}^{\mathbf{n_x} \times (\mathbf{n_x}+\mathbf{n_c})}$ such that the inequality (29) is verified. In such an event, the dynamical controller $\mathbf{K_a}(\rho) = \mathbf{G_a^{-1}L_a}(\rho)$ stabilises the error system (17) asymptotically for all matrices $\tilde{\mathbf{A}}(\rho)$ described as a convex combination of the elements in $\mathcal{A}$.*

1. *Find $\tilde{\mathbf{P}}$ and $\tilde{\mathbf{F}}_\mathbf{0}(\rho)$ that satisfy the following LMIs*

$$\tilde{\mathbf{P}} = \tilde{\mathbf{P}}^\mathbf{T} > \mathbf{0} \quad (27)$$

$$\tilde{\mathbf{P}}\tilde{\mathbf{A}}_\mathbf{0j} + \tilde{\mathbf{A}}_\mathbf{0j}^\mathbf{T}\tilde{\mathbf{P}} < \mathbf{0}, \quad (28)$$

where $j = 1 \dots 2^M$ and $\tilde{\mathbf{A}}_\mathbf{0j} = \tilde{\mathbf{A}}_\mathbf{gj} + \tilde{\mathbf{B}}_\mathbf{gj}\tilde{\mathbf{F}}_\mathbf{0j}$; $\tilde{\mathbf{F}}_\mathbf{0j}$: a state feedback matrix which stabilizes the following system $\tilde{\mathbf{G}}$,

2. *With $\tilde{\mathbf{P}}$ and $\tilde{\mathbf{F}}_\mathbf{0}(\rho)$, find the accompanying controller $\mathbf{K_a}(\rho)$ solution of the following LMI*

$$\begin{bmatrix} \tilde{\mathbf{A}}_\mathbf{0j}^\mathbf{T}\tilde{\mathbf{P}} + \tilde{\mathbf{P}}\tilde{\mathbf{A}}_\mathbf{0j}^\mathbf{T} & \tilde{\mathbf{P}} & \mathbf{0} \\ \tilde{\mathbf{P}} & \mathbf{0} & \mathbf{0} \\ \mathbf{0} & \mathbf{0} & \mathbf{0} \end{bmatrix}$$
$$+ Sym\left\{ \begin{bmatrix} \mathbf{F1} \\ \mathbf{F2} \\ 0 \end{bmatrix} \begin{bmatrix} \mathbf{0} & -\mathbf{I} & \tilde{\mathbf{B}}_\mathbf{g} \end{bmatrix} \right\}$$
$$+ Sym\left\{ \begin{bmatrix} \mathbf{0} \\ \mathbf{0} \\ \mathbf{I} \end{bmatrix} \begin{bmatrix} \mathbf{L_{aj}}\tilde{\mathbf{C}}_\mathbf{g} - \mathbf{G_a}\tilde{\mathbf{F}}_\mathbf{0j} & \mathbf{0} & -\mathbf{G_a} \end{bmatrix} \right\} < 0, \quad (29)$$

where $j = 1 \dots 2^M$ and $\mathbf{F1}$, $\mathbf{F2}$ are non-zero matrices and matrices $\mathbf{G_a}$ and $\mathbf{L_{aj}}$ are such that $\mathbf{K_{aj}} = \mathbf{G_a^{-1}L_{aj}}$.
3. *Obtain a realization of the controller $\mathbf{K}(\omega_0)$ via (20).*

Some details of the illustrated approach can be found in [9] and in [33].

Proof.
In order to verify the existence of $\mathbf{K}(\omega_0)$ satisfying Proposition 1, the conditions of (18) and (19) could be proved by referring

to Lemma 1. An LMI solution is proposed for designing the controller $\mathbf{K_a}$ that ensures quadratic stabilisation. This condition is at the origin of the Bilinear Matrix Inequalities (BMIs). However, it is possible to transform it into a set of LMIs using the projection lemma (see [9]). This approach relies on the application of a dynamic feedback control solution, which is then converted into a static output feedback control problem. Let

$$\begin{aligned} \tilde{A}_f &= \tilde{A}_g + \tilde{B}_g\tilde{F}_0 - \tilde{B}_g\tilde{F}_0 + \tilde{B}_g K_a \tilde{C}_g \\ &= \tilde{A}_0 + \tilde{B}_g\left(K_a\tilde{C}_g - \tilde{F}_0\right) \end{aligned} \tag{30}$$

by applying the projection lemma, the equation (25) becomes equivalent to

$$\begin{aligned} &\begin{bmatrix} \tilde{A}_0^T\tilde{P} + \tilde{P}\tilde{A}_0 & \tilde{P} \\ \tilde{P} & 0 \end{bmatrix} \\ &+ Sym\left\{\begin{bmatrix} F1 \\ F2 \end{bmatrix}\begin{bmatrix} 0 & -I \end{bmatrix}\right\} \\ &+ Sym\left\{\begin{bmatrix} F1\tilde{B}_g \\ F2\tilde{B}_g \end{bmatrix}\begin{bmatrix} K_a\tilde{C}_g - \tilde{F}_0 & 0 \end{bmatrix}\right\} < 0 \end{aligned}$$

which can be written as

$$\begin{aligned} &\begin{bmatrix} \tilde{A}_0^T\tilde{P} + \tilde{P}\tilde{A}_0 & \tilde{P} & 0 \\ \tilde{P} & 0 & 0 \\ 0 & 0 & 0 \end{bmatrix} \\ &+ Sym\left\{\begin{bmatrix} F1 \\ F2 \\ 0 \end{bmatrix}\begin{bmatrix} 0 & -I & 0 \end{bmatrix}\right\} \\ &+ Sym\left\{\begin{bmatrix} F1\tilde{B}_g \\ F2\tilde{B}_g \\ 0 \end{bmatrix}\begin{bmatrix} 0 & 0 & I \end{bmatrix}\right\} \\ &+ Sym\left\{\begin{bmatrix} 0 \\ 0 \\ I \end{bmatrix} G\begin{bmatrix} K_a\tilde{C}_g - \tilde{F}_0 & 0 & -I \end{bmatrix}\right\} < 0 \end{aligned} \tag{31}$$

which corresponds to the condition (29) of the theorem which has been expressed on the vertices of the polytope, see (24).

Inequality (31) holds if

$$\begin{aligned} &\begin{bmatrix} \tilde{A}_0^T\tilde{P} + \tilde{P}\tilde{A}_0 & \tilde{P} \\ \tilde{P} & 0 \end{bmatrix} \\ &+ Sym\left\{\begin{bmatrix} F1 \\ F2 \end{bmatrix}\begin{bmatrix} 0 & -I \end{bmatrix}\right\} < 0 \end{aligned} \tag{32}$$

Using the projection lemma, inequality (32) is equivalent to

$$\tilde{P}\tilde{A}_0 + \tilde{A}_0^T\tilde{P} < 0, \tag{33}$$

which corresponds to the first statement of the theorem. ■

6 Simulation results

The HEV powertrain test simulator is composed of a mono-cylinder diesel engine and a parallel-flywheel type of motor/generator. The configuration of the simulator is based on the experimental platform, which is represented in Fig. 6 and the characteristics of which are provided in Tab. 1.

The complexity of the tests carried out in this study, in particular, the use of a speed observer, a speed reference trajectory, and diesel engine torque varying with time, meant that it was impractical to carry out these experiments. Indeed, the bench shown in Fig. 6 is a stationary bench and the PMSM drive does not allow the integration of a sensorless observer. This is the reason why it was decided to conduct a simulation. However, the models used in the simulator were validated and are representative of the actual behaviour of the experimental bench. Although this platform consists of a single-cylinder diesel combustion engine it would be easy to extend the results to three- or four-cylinder engines. In this case the harmonics would have different frequencies and amplitudes as represented in Fig. 2. The overall scheme is described in Fig. 3.

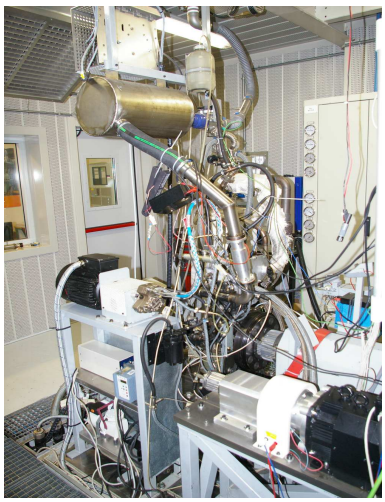

Fig. 6: HEV Experimental platform

Hybrid powertrain Descriptions	Specification
Diesel engine	499cm3 65 kW and 190 Nm
PMSM Motor/generator	15kW, 64Nm/2100rpm
IM (Induction Motor) dynamometer	47kw-1700rpm
Injection timing	$\mathbf{600}\mu s$
diesel flow	13.3mg/injection
rail pressure	700 bar

Table 1 Hybrid powertrain specifications

The speed trajectory of the PMSM-combustion engine assembly is shown in Fig. 7. The corresponding load torque has been represented in Fig. 8. The scheme represents an urban start-up and shut-down cycle. The design of the controller was based on three harmonics and the numerical value of the controller can be found in the appendix. In Fig. 9-10, a comparison is made between our

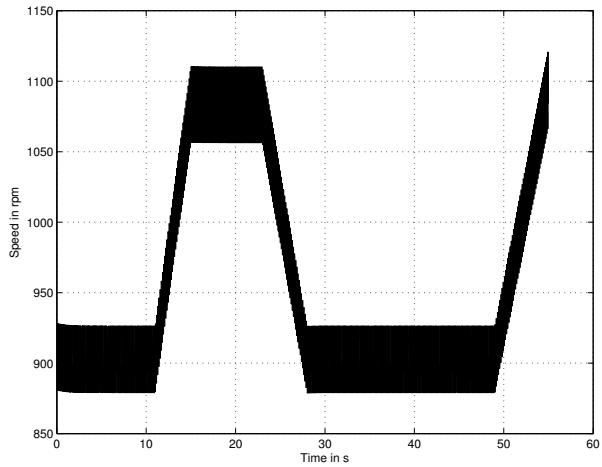

Fig. 7: Thermal engine speed reference

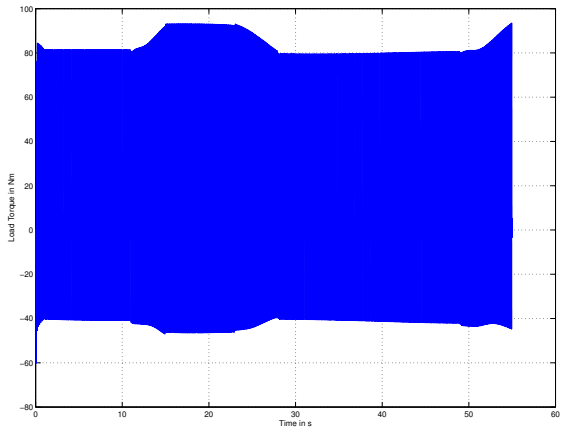

Fig. 8: Load Torque

observer and that of [20] which is another type of nonlinear observer. The results are similar and the estimation error is slightly lower in our case. the output of the position/speed estimator presented in this paper compares well with the measured speed. The error remains low and the estimator follows the trajectory well in the frame of speed dynamic variations.

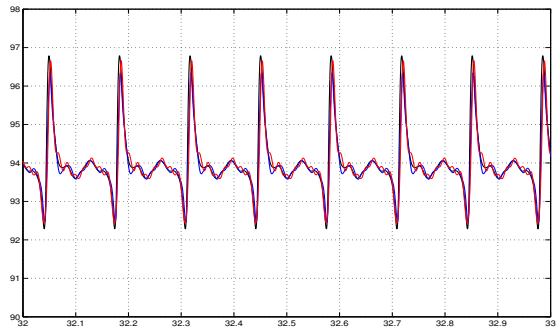

Fig. 9: Zoom of estimated speed error comparison : black = mesured; blue= our approach; red= [20]

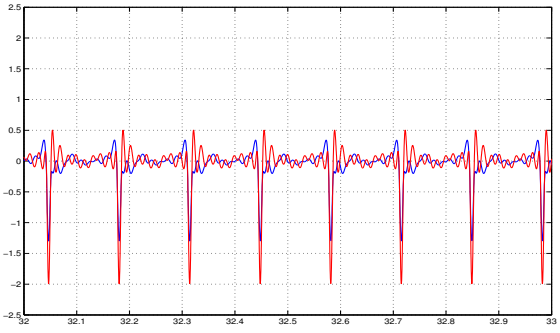

Fig. 10: Zoom of estimated speed error comparison :blue= our approach; red= [20]

A recursive least mean square algorithm is used to estimate all speed ripple harmonics. As a consequence, a reference trajectory y_{ref} can be generated without the unwanted harmonics. The results concerning the attenuation of the first three harmonics of speed are illustrated in Fig. 11.

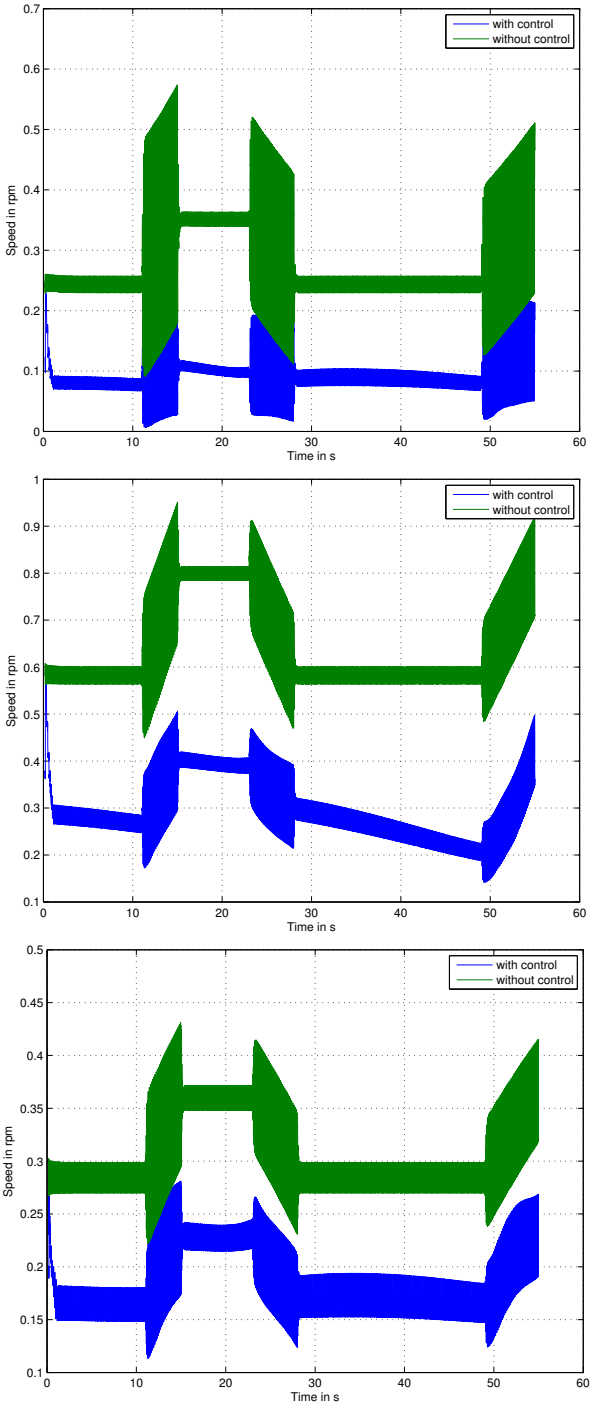

Fig. 11: 1st speed harmonic (top), 2nd harmonic (middle), 3rd harmonic(bottom) green without control; blue with control.

The chattering present in the results is mainly due to the harmonic behaviour of the reference trajectories. Even though it is possible to attenuate more than three harmonics, we chose to attenuate the three most energetic and most troublesome (low frequency) harmonics. We set the value of the coefficient $\kappa = 0.25$ of Proposition 1 to prevent the harmonics from being completely attenuated. This is because of the electrical power available in the PMSM. The presented strategy correctly attenuates the set of torque ripples generated by the combustion engine. The ripple attenuation is made considering the energy consumption and electrical power available.

7 Conclusion

This paper presents an original attenuation solution for torque ripples occurring in a combustion engine in the configuration of a hybrid electric vehicle. The approach is based on an observer that does not require the measurement of the torque, speed, or position. An LPV output regulation strategy is added to meet the overall requirements for mitigating the torque disturbance over a wide range of speed variations. A simulation was then carried out to validate the proposed approach. The advantage of this method is that it does not require a nonlinear model of the system generating the disturbance (here a diesel engine). In this case the system is considered as a non-stationary multi-sinusoidal perturbation generator. This methodology can be easily extended to all systems generating sinusoidal or pulsed signals such as a diesel power generators or wind turbines. From the perspective of future work, the LPV control should be improved by optimising the synthesis on different parameter domains (in this case the speed). Another original approach would be to use observers with unknown inputs to estimate the multi-sinusoidal disturbance.

8 References

1 J. Chauvin, G. Corde, P. Moulin, M. Castagne, N. Petit, and P. Rouchon, "Time-varying linear observer for torque balancing on a di engine," in *IFAC Symposium on Advances in Automotive control*, April 19-23 2004.

2 A. Preumont, "Vibration control of active structures : An introduction," *Springer*, 2011.

3 S. V. Gusev, W. Johnson, and J. Miller, "Active flywheel control based on the method of moment restriction," in *American Control Conference*, 1997.

4 Y. Nakajima, M. Uchida, H. Ogane, and Y. Kitajima, "A study on the reduction of crankshaft rotational vibration velocity by using a motor-generator," *JSAE Review*, vol. 21, pp. 335–341, 2000.

5 R. I. Davis and R. D. Lorenz, "Engine torque ripple cancellation with an integrated starter alternator in a hybrid electric vehicle," *Implementation and control, IEEE Transactions on Industry Applications*, vol. 39, pp. 1765 – 1774, 2003.

6 M. Beuschel and D. Schroder, "Adaptive damping of torque pulsation using a starter generator -opportunities and boundaries," *Industry Applications Conference IEEE*, vol. 3, pp. 1403 – 1408, 2000.

7 P. Micheau and P. Coirault, "A harmonic controller of engine speed oscillations for hybrid vehicles," in *16th World IFAC Congress, Automotive Control, Prague, Czech Republic.*, 2005.

8 M. Njeh, S. Cauet, P. Coirault, and P. Martin, "H_∞ control strategy of motor torque ripple in hybrid electric vehicles: an experimental study," *IET Control Theory Applications*, vol. 5, no. 1, pp. 131–144, January 2011.

9 M. Njeh, S. Cauet, and P. Coirault, "LPV control of ICE torque ripple in hybrid electric vehicles," in *World IFAC*, Milano, Italy, 28 August - 02 September 2011.

10 R. S. Vadamalu and C. Beidl, "Mpc for active torsional vibration reduction of hybrid electric powertrains," *Int. Symposium on Advances in Automotive Control*, 2016.

11 C. Yang, X. Jiao, L. Li, Y. Zhang, L. Zhang, and J. Song, "Robust coordinated control for hybrid electric bus with single-shaft parallel hybrid powertrain," *IET Control Theory Applications*, vol. 9, no. 2, pp. 270–282, 2015.

12 M. Morandin, S. Bolognani, A. Pevere, S. Calligaro, and R. Petrella, "Active torque ripple damping in direct drive range extender applications: A comparison and an original proposal," in *2015 IEEE Vehicle Power and Propulsion Conference (VPPC)*, Oct 2015, pp. 1–6.

13 Q. Wang, K. Rajashekara, Y. Jia, and J. Sun, "A real-time vibration suppression strategy in electric vehicles," *IEEE Transactions on Vehicular Technology*, vol. PP, no. 99, pp. 1–1, 2017.

14 M. Morandin, S. Bolognani, and A. Faggion, "Active torque damping for an ice-based domestic chp system with an spm machine drive," *IEEE Transactions on Industry Applications*, vol. 51, no. 4, pp. 3137–3146, July 2015.

15 H. Kubota and K. Matsuse, "Dsp-based speed adaptive flux observer of induction motor," *IEEE Trans Ind Appl*, vol. 29, pp. 344–348, 1993.

16 M. Hinkkanen, M. Harnefors, and J. Luomi, "Reduced-order flux observers with stator-resistance adaptation for speed-sensorless induction motor drives," *IEEE Trans Power Electron*, vol. 25, pp. 1173–1183, 2010.

17 D. Xu, S. Zhang, and J. Liu, "Very-low speed control of pmsm based on ekf estimation with closed loop optimized parameters," *ISA Trans*, vol. 52, pp. 835–843, 2013.

18 T. Orlowska-Kowalska and M. Dybkowski, "Stator-current-based mras estimator for a wide range speed-sensorless induction-motor drive," *IEEE Trans. Ind. Electron.*, vol. 57, pp. 1296–1308, 2010.

19 J. Shigley, J. Uicker, and G. Pennock, *Theory of Machines and Mechanisms*, 3rd ed. New York, Oxford University Press, 2003.

20 J. Lee, J. Hong, K. Nam, and R. Ortega, "Sensorless control of surface-mount permanent-magnet synchronous motors based on a nonlinear observer," *IEEE Trans. Power Electronics*, vol. 25, no. 2, pp. 290–297, 2010.

21 A. Piippo, M. Hinkkanen, and J. Luomi, "Analysis of an adaptive observer for sensorless control of interior permanent magnet synchronous motors," *IEEE Trans. Industrial Electronics*, vol. 55, no. 3, pp. 570–576, Feb. 2008.

22 T. Tuovinen, M. Hinkkanen, L. Harnefors, and J. Luomi, "Comparison of a reduced-order observer and a full-order observer for sensorless synchronous motor drives," *Implementation and control, IEEE Transactions on Industry Applications*, vol. 48, no. 6, pp. 1959–1967, 2012.

23 M. L. Masmoudi, E. Etien, S. Moreau, and A. Sakout, "Amplification of single mechanical fault signatures using full adaptive pmsm observer," *IEEE Trans. Industrial Electronics*, vol. 64, no. 1, pp. 615–623, 2017.

24 A. Piippo, M. Hinkkanen, and J. Luomi, "Adaptation of motor parameters in sensorless pmsm drives," in *7th International Conference on Power Electronics and Drive Systems (PEDS)*, Bangkok, Thailand, November 2007, pp. 1301–1306.

25 H. Luo, Q. Yin, X. Li, and Y. Liu, "An improved adaptive observer for permanent magnet synchronous motor," in *9th Conf. IEEE Industrial Electronics and Applications*

ICIEA, Hangzhou, China, June 2014, pp. 1301–1306.

26 T. Hua, A. R. Teel, and Z. Lin, "Lyapunov characterization of forced oscillations," *Automatica*, vol. 41, pp. 1723 –1735, 2005.

27 P. Apkarian, P. Gahinet, and G. Beker, "Self-scheduled $\mathcal{H}_\infty$ control of linear parameter-varying systems: A design example," *Automatica*, vol. 31, no. 9, pp. 1251–1262, 1995.

28 P. Apkarian and P. Gahinet, "A convex characterization of gain scheduled $\mathcal{H}_\infty$ controllers," *IEEE Transaction on Automatic Control*, vol. 40, no. 5, pp. 853–864, 1995.

29 A. Packard, "Gain scheduling via linear fractional transformations," *Systems and Control Letters*, vol. 22, no. 2, pp. 79–92, 1994.

30 H. Koroglu and C. W. Scherer, "An LMI approach to $\mathcal{H}_\infty$ synthesis subject to almost asymptotic regulation constraints," *Systems and Control Letters*, vol. 57(4), pp. 300–308, 2008.

31 C. W. Scherer, P. Gahinet, and M. Chilali, "Multiobjective output-feedback control via lmi optimization," *IEEE Trans. Automat Control*, vol. 42 (7), pp. 896–911, 1997.

32 C. W. Scherer, "Linear parameter varying control and full block multipliers," *Automatica*, vol. 37, pp. 361–375, 2001.

33 F. Barbagli, G. Marro, P. Mercorelli, and D. Prattichizzo, "Some results on output algebraic feedback with applications to mechanical systems," in *Proceedings of the 37th IEEE Conference on Decision and Control (Cat. No.98CH36171)*, vol. 3, 1998, pp. 3545–3550 vol.3.

9 Appendix: Controller Numerical Values

For the operating point ω_0 For the controller K_i:

$$K_i = \begin{bmatrix} 0 & 102 & 0 & 0 & 0 & 0 \\ -102 & 0 & 0 & 0 & 0 & 0 \\ 0 & 0 & 0 & 204 & 0 & 0 \\ 0 & 0 & -204 & 0 & 0 & 0 \\ 0 & 0 & 0 & 0 & 0 & 306 \\ 0 & 0 & 0 & 0 & -306 & 0 \end{bmatrix}$$

For the controller K_a:

$$A_{ca0} = \begin{bmatrix} -9.5187 & 0.2145 & 0.3869 & 0.2875 \\ 0.2126 & -9.9053 & 0.1707 & 0.1270 \\ 0.3547 & 0.1581 & -9.7149 & 0.2119 \\ 0.2956 & 0.1316 & 0.2375 & -9.8234 \end{bmatrix}$$

$$B_{ca0} = \begin{bmatrix} 0.0974 \\ 0.0432 \\ 0.0714 \\ 0.0616 \end{bmatrix}$$

$$C_{ca0} = 1e^3 * \begin{bmatrix} -0.3804 & -0.1695 & -0.2796 & -0.2300 \\ -0.0484 & -0.0216 & -0.0354 & -0.0294 \\ -0.9221 & -0.4106 & -0.6786 & -0.5587 \\ 0.2433 & 0.1084 & 0.1789 & 0.1469 \\ -1.5863 & -0.7061 & -1.1674 & -0.9613 \\ 0.3933 & 0.1751 & 0.2895 & 0.2376 \\ -0.0046 & -0.0017 & -0.0031 & -0.0028 \end{bmatrix}$$

$$D_{ca0} = 1e^3 * \begin{bmatrix} -0.1326 \\ -0.0207 \\ -0.3088 \\ 0.0494 \\ -0.4648 \\ -0.0290 \\ 1.1083 \end{bmatrix}$$

For Γ:

$$\Gamma_0 = \begin{bmatrix} -0.0008 \\ 0.3059 \\ -0.0059 \\ 0.2903 \\ -0.0181 \\ 0.2678 \end{bmatrix}^T$$

For the variation around this operating point : For the controller K_i:

$$K_i = \begin{bmatrix} 0 & 1 & 0 & 0 & 0 & 0 \\ -1 & 0 & 0 & 0 & 0 & 0 \\ 0 & 0 & 0 & 2 & 0 & 0 \\ 0 & 0 & -2 & 0 & 0 & 0 \\ 0 & 0 & 0 & 0 & 0 & 3 \\ 0 & 0 & 0 & 0 & -3 & 0 \end{bmatrix}$$

For the controller K_a:

$$A_{ca1} = 1e^{-3} * \begin{bmatrix} 0.1032 & -0.0083 & -0.0205 & 0.0037 \\ 0.0438 & -0.0025 & -0.0056 & 0.0016 \\ 0.0737 & -0.0046 & -0.0111 & 0.0027 \\ 0.0667 & -0.0035 & -0.0097 & 0.0022 \end{bmatrix}$$

$$B_{ca1} = 1e^{-5} * \begin{bmatrix} -0.6328 \\ -0.2805 \\ -0.4667 \\ -0.3885 \end{bmatrix}$$

$$C_{ca1} = 1e^{-3} * \begin{bmatrix} -2.2 & 0.747 & 0.173 & -0.32 \\ -0.822 & -0.534 & -0.0666 & -0.133 \\ -2.118 & 0.427 & 1.1590 & -0.098 \\ 1.588 & -0.837 & -1.1576 & -0.621 \\ -5.253 & -0.277 & -2.2470 & -1.809 \\ -1.37 & -0.626 & -1.3654 & -1.367 \\ -0.0070 & -0.0036 & 0.0083 & 0.0009 \end{bmatrix}$$

$$D_{ca1} = 1e^{-4} \begin{bmatrix} 2.43 \\ -1.48 \\ 5.80 \\ -3.75 \\ 14.45 \\ -6.17 \\ 0.023 \end{bmatrix}$$

For Γ:

$$\Gamma_0 = 1^{e-3} * \begin{bmatrix} -0.0147 \\ -0.0893 \\ -0.1103 \\ -0.3321 \\ -0.3355 \\ -0.6673 \end{bmatrix}^T$$